Modeling and Identification of Electromechanical Actuators for the ILR-33 AMBER Rocket

Jan Kierski, Hubert Graczyk
Lukasiewicz Research Network – Institute of Aviation, Aleja Krakowska 110/114, 02-256 Warsaw

Abstract: The aim of the work was to develop a method for modeling, testing, and identifying electromechanical actuators for rocket applications. Works were performed using a prototype solution designed for the ILR-33 AMBER suborbital rocket, developed by Łukasiewicz Research Network – Institute of Aviation. A set of physical relationships was used to create system's mathematical model, including Kirchhoff's laws, Newton's laws, and nonlinear friction models. System's tests were then performed. A new method of results analysis was applied herein to gather unknown parameters for the model and to confirm an elevated level of convergence between both model and experiment in all cases analyzed. The identification approach proved itself to be effective and useful. A complex approach concerning modeling, testing and identification of such actuators was explained for the first time in this paper. The methods presented herein can be applied in other disciplines, wherever electromechanical actuator systems are used, and where their proper identification is necessary to ensure system reliability and safety. Presented solutions are simple to implement, and the test stands do not require expensive measurement equipment. The results obtained permit to create a high-fidelity model at a reasonably low computational cost.

Keywords: Suborbital rocket, ILR-33 AMBER, modeling, identification, electromechanical actuator, servo drive, control system

1. Introduction

In 2014, the ILR-33 AMBER suborbital rocket project was launched at the Łukasiewicz Research Network - Institute of Aviation. The aim of the project is to develop a technology demonstrator, utilizing a hybrid motor with an environmentally friendly oxidizer – HTP (*High-Test Peroxide*) [1]. The rocket is designed to reach an apogee exceeding 100 km with a payload of 10 kg [2]. However, the execution of unguided rocket flights at such apogees in most of the countries, including Poland is not currently possible. The calculated dispersion of the landing point is of dozens of kilometers and is too elevated to meet the flight safety requirements of landing of all rocket components inside the permitted area. This currently forces high apogee rocket launches to be carried out from very few ranges, which occupancy is elevated and involves high costs and complicated organization of launch campaigns [3].

The decision was therefore taken to develop an active flight control system to compensate trajectory disturbances in the initial phase of flight, thereby significantly reducing the dispersion of the impact point. Based on the analysis presented in a study entitled „Polish Suborbital Capabilities", prepared in 2021 by ILOT for the Polish Space Agency, such solution would permit to execute flights from the Polish coast at apogees above 100 km. This would significantly increase the amount of possible research activities conducted on national training grounds [4]. It has been assumed that such a control system should consist of a set of sensors measuring the current flight parameters, algorithms analyzing data from these sensors and calculating control commands based on them, and an actuation system executing these commands and therefore influencing the flight trajectory.

This article focuses on the mathematical modeling, simulating, and testing a prototype solution of the mentioned actuation system. During the concept design phase, which is out of scope of this article, a preliminary design of the system was developed. The system is built in a canard aerodynamic configuration and can be installed as an additional module directly under the nosecone of the rocket. The currently developed version of the system is envisaged to be used on the ILR-33 AMBER rocket. The system consists of:

- Four servo drives connected to the canards. Servo drives are composed of an off-the-shelf BLDC (*Brushless Direct Current*) motor, a two-stage gear train and an incremental encoder on the motor shaft. Addition of an absolute encoder on the canard shaft is planned in the next version of the system;
- Four off-the-shelf motion controllers, on which torque, velocity and position control algorithms are implemented. The motion controllers are attached to an interface PCB

Autor korespondujący:
Jan Kierski, jan.kierski@ilot.lukasiewicz.gov.pl

Artykuł recenzowany
nadesłany 08.04.2024 r., przyjęty do druku 08.07.2024 r.

(*Printed Circuit Board*), which manages signals routing, power distribution and facilitates mechanical integration;
— A Li-ion battery – source of electrical power;
— Other structural mechanical and electrical components.

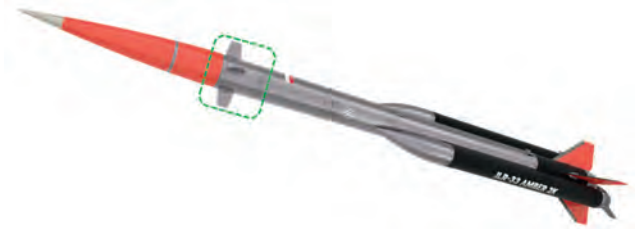

Fig. 1. Visualization of the guided version of the ILR-33 AMBER rocket – the control system in marked with a green dashed box
Rys. 1. Wizualizacja sterowanej wersji rakiety ILR-33 BURSZTYN – system sterowania oznaczono zieloną przerywaną ramką

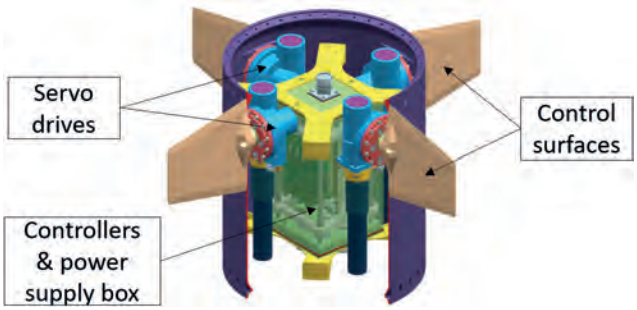

Fig. 2. 3D CAD model of the control system prototype version
Rys. 2. Model 3D CAD prototypowej wersji systemu sterowania

A view of the system integrated with the rocket is shown in Fig. 1. A CAD (*Computer Aided Design*) model of the prototype version of the system is shown in Fig. 2.

Mathematical models of similar systems have been broadly described in the literature. They were implemented and used among other in the development of HiL (*Hardware-in-the-Loop*) simulations for guided missiles [5], or for GNC algorithms development purposes [6]. However, models presented in the literature differs considerably in terms of complexity, from simple transmittance equations [5], via moderate complexity models [6, 7], up to very high fidelity representations, including for example complex friction models, nonlinearities and backlash or internal motor phase currents modeling [8, 9]. As it was noticed in [10], the chosen modeling complexity is a trade-off between the desired fidelity level, accessible computing power and the time spent by the system designers. For the case described below, a dedicated approach was developed to provide an accurate representation of the system dynamics at a relatively low computability cost. This was dictated by the main purpose of the model, which was the electromechanical actuator qualification for flight and the use in flight simulations during MiL (*Model-in-the-Loop*) experiments.

Test stands approach for similar systems' components was demonstrated in various sources [6, 8, 11]. In the case below, main efforts were put on tests that would permit the collection of unknown parameters for the mathematical model, its' comparison to experimental results and components qualification for flight. A new method of results analysis to gather unknown parameters for the model was presented herein. The effort was also put to minimize the development of dedicated test hardware and software and make use of accessible off-the-shelf solutions.

In the next chapters, a complex approach was shown, including mathematical modeling, performing bench testing, data correlation methods and verification of obtained results. The aim of these activities was not only to qualify the prototype solution, but also to establish and standardize the workflow allowing design evaluation, optimization and stand qualification of similar systems.

2. Mathematical modeling

2.1. Method and assumptions

A mathematical model of the control system was created. The model consists of a set of equations describing the behaviour of its components and of logical relationships between them. It was assumed that:
— all the equations of motion should be based on verified physical laws and models.
— all the unknown physical values of the model should be verifiable, firstly using experimental tests and secondly using manufacturers' catalogue data.

A set of simplifying assumptions was also introduced:
— external loads and accelerations of the rocket (except canard hinge moment) does not affect the system performance.
— no backlash and elasticities exist in the mechanical elements (elements are stiff)
— the motor and gears have symmetrical mechanical and electrical characteristics in both rotation directions.

2.2. Motion controller modeling

A Faulhaber MC5004P motion controller is used in the system. The controller behavior was modeled based on the manufacturer's user manual [14]. The controller has a processor-implemented classical three-stage control algorithm, consisting of feedback loops and a separate power electronics module.

The external loop is responsible for the angular position control and consists of a proportional controller. The middle and inner loop are responsible for controlling respectively the angular velocity and motor current (proportional to the motor torque) and have PI-type controllers implemented. A set of constrains is also included in the model, such as maximum speed, acceleration, and peak current values, consistent with hardware limitations.

A fourth control loop on the motor controller exists and is responsible for adjusting the PWM (*Pulse Width Modulation*) signal, which corresponds the effective voltage on each of the three motor phases. Due to the method adopted for modeling the BLDC motor, this loop has been intentionally omitted, as it is not necessary for the correct operation of the model. A general system diagram is shown in Fig. 3.

Fig. 3. Control loops implemented on the motion controller
Rys. 3. Pętle sterowania zaimplementowane na kontrolerze ruchu

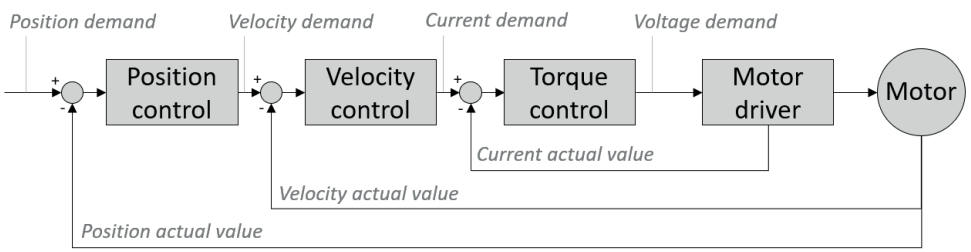

Due to the aforementioned modeling way, the settings of the control loops in the model and on the real motion controller correspond directly to each other. This allows the settings of the motion controller to be tested and optimized with the use of numerical simulations, without performing multiple test runs on real hardware.

2.3. Electrical motor modeling

The BLDC motor is considered as a torque source for the servo drive. A Faulhaber 2264W012BP4 motor have been used in the system [15]. The motor was modeled using Kirchhoff's law, in a manner analogous to that presented in the article [7]. Thus, we have (1):

$$U_{motor}\left(t\right) = k_E \cdot \omega_{motor}\left(t\right) + I_{motor}\left(t\right) \cdot R + L \cdot \frac{dI_{motor}\left(t\right)}{dt} \tag{1}$$

where U_{motor} is the effective voltage applied on the motor, I_{motor} is the motor current, k_E is the back-EMF (electromotive force) constant, R is the phase-phase terminal resistance, L is the phase-phase terminal inductance, and ω_{motor} is the actual motor angular velocity.

The electrical torque generated by the motor can be also described by the following equation (2):

$$M_{motor.el} = k_M \cdot I_{motor}\left(t\right) \tag{2}$$

where k_M is the torque constant of the motor.

After transformation the equations mentioned above, we obtain a formula (3) for the torque generated by the motor depending on the voltage applied, its actual state and physical parameters:

$$M_{motor.el} = \frac{k_M}{R}\left(U_{motor}\left(t\right) - k_E \cdot \omega_{motor}\left(t\right) - L \cdot \frac{dI_{motor}\left(t\right)}{dt}\right) \tag{3}$$

2.4. Mechanical elements modeling

The mechanical friction torque of the motor was modeled using the Coulomb friction model [12]. The friction is described by two parameters, the static and dynamic coefficient (respectively $C_{0.motor}$ and $C_{v.motor}$) and has a following formula (4):

$$M_{motor.mech} = C_{0.motor} \cdot \mathrm{sgn}\left(\omega_{motor}\right) + C_{v.motor} \cdot \omega_{motor} \tag{4}$$

As it can be seen, there is a discontinuity in the friction model at $\omega_{motor} = 0$, corresponding to the static friction case.

There are two mechanical gearboxes in the system: a Faulhaber 26/1R planetary gearbox with a reduction ratio of $i_{plan} = 66:1$ [16] and a custom made self-locking angular gearbox with a reduction rate of $i_{worm} = 36:1$. They are connected in series so that the output shaft of the planetary gearbox is the input shaft of the angular gearbox. The mechanical torque resulting from the internal friction of the two gears is modeled in the same way as for the motor. Thus, we have (5), (6):

$$M_{plan} = C_{0.plan} \cdot \mathrm{sgn}\left(\omega_{motor}\right) + C_{v.plan} \cdot \omega_{motor} \tag{5}$$

$$M_{worm} = C_{0.worm} \cdot \mathrm{sgn}\left(\omega_{motor}\right) + C_{v.worm} \cdot \omega_{motor} \tag{6}$$

where $C_{0.plan}$, $C_{v.plan}$, $C_{0.worm}$, and $C_{v.worm}$ are respectively static and dynamic friction coefficients of each of the gearboxes.

All of the coefficients are intentionally determined in relation to the motor angular velocity ω_{motor}. This approach facilitates the comparison of experimental results with the model and allows a quick assessment of each gear friction influence on the entire system dynamics. However, it requires rescaling of the coefficients or re-identification of the system if any of the gears changes.

During the flight, the rocket body is subjected to varying external loads, which depend on the actual velocities and accelerations, Mach number, aeroballistic angles, canard deflection angles and (to a lesser extent) other factors [13]. A complete model of all loads acting on the ILR-33 AMBER rocket was obtained from aerodynamic analyses and flight ballistics simulations and is not the subject of this paper. For the purpose of the analyses presented here, it was assumed that only the canard hinge moment M_{ext} has a significant influence on the control system's dynamics. This moment, depending on the flight state, varies between 0 and ±8 Nm. For the servo drive it is a source of additional friction occurring on the components, primarily on the gearing teeth and the ball bearings. It was assumed that the additional friction value is proportional to the absolute value of the applied external torque and that it will always counteract the movement of the gears. On this basis, a formula (7) for the friction moment value was obtained:

$$M_{canard} = C_{M.canard} \cdot \left|M_{ext}\right| \cdot \mathrm{sgn}\left(\omega_{motor}\right) \tag{7}$$

where $C_{M.canard}$ is an empirically determined friction coefficient.

Once all the components of the friction torque in the system have been determined, we can obtain the formulas (8), (9) for its total value:

$$M_{mech} = M_{motor.mech} + M_{plan} + M_{worm} + M_{canard} \tag{8}$$

$$M_{mech} = C_0 \cdot \mathrm{sgn}\left(\omega_{motor}\right) + C_v \cdot \omega_{motor} + C_M \cdot \left|M_{ext}\right| \cdot \mathrm{sgn}\left(\omega_{motor}\right) \tag{9}$$

where C_0, C_v, and C_M are determined for the whole servo drive and are the sum of all the corresponding components values.

A graphical representation of the equation is shown on Fig. 4.

Once the model is defined, mechanical system identification issue is reduced to determining the values of the coefficients C_0, C_v, and C_M.

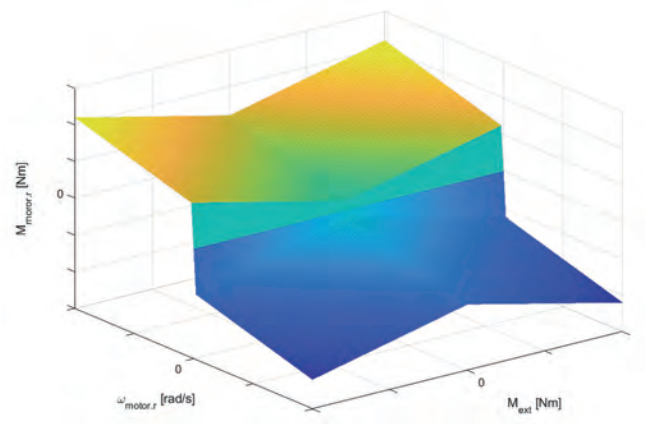

Fig. 4. Assumed friction torque model of the servo drive
Rys. 4. Założony model momentu tarcia serwomechanizmu

2.5. Equations of motion

Since the electromechanical actuator, consisting of the motor, the two gearboxes and the canard, is mechanically connected, its equations of motion must be considered together. It was decided that the equations would be solved in relation to the motor shaft, but it is also possible to define analogous equations for the intermediate shaft and the output shaft of the gearboxes, the solution of which would lead to identical results. The equations are defined based on Newton's second law for rotational motion (10):

$$\varepsilon_{motor}\left(t\right) = \frac{M_{eqiv}\left(t\right)}{J_{eqiv}} \tag{10}$$

where M_{eqiv} is the total equivalent moment on the motor shaft.

This moment can be obtained by summing all of its components, determined in previous chapters. Since all moments are determined with reference to the motor velocity, it is possible to sum them directly (11):

$$M_{eqiv}\left(t\right) = M_{motor.el} - M_{mech} \tag{11}$$

J_{eqiv} is the equivalent moment of inertia with reference to the motor shaft and can be calculated using the formula (12):

$$J_{eqiv} = J_{motor} + J_{plan.in} + \frac{J_{plan.out} + J_{worm.in}}{i_{plan}^2} + \frac{J_{worm.out} + J_{canard}}{i_{plan}^2 \cdot i_{worm}^2} \tag{12}$$

Each rotating component moments of inertia J are determined from manufacturers' datasheets or their 3D CAD models. For elements located on the intermediate axis between the gearboxes and on the canard shaft, it is necessary to scale them by the squares of the corresponding gear ratios.

Knowing the motor shaft acceleration, it is possible to determine its angular velocity (13) and position (14) in time:

$$\omega_{motor}\left(t\right) = \omega_{motor.0} + \int_0^t \varepsilon_{motor} dt \tag{13}$$

$$\delta_{motor}\left(t\right) = \delta_{motor.0} + \int_0^t \omega_{motor} dt \tag{14}$$

Resulting values can be scaled by the gear ratios, and thus acceleration, speed and position of the canard shaft can be obtained.

2.6. Model implementation

Mathematical equations were implemented in the MATLAB/Simulink environment. The resulting model consists of a set of scripts for loading constants and initial settings and a Simulink model in which simulations are performed iteratively. A view of the Simulink model is shown in Fig. 5. In order to eliminate discontinuities in the equations and improve the stability of the numerical solution, all $\mathrm{sgn}\left(\omega\right)$ functions were replaced by $\tanh\left(\omega\right)$.

3. Test stand identification

The control system loops were tuned to obtain optimal system dynamics and required margins of stability (which is out of scope of this paper). Then, a set of identification tests was performed with the aim to obtain unknown C_0, C_v, and C_M coefficients and to complete the mathematical model on their basis. To perform it, a test plan was implemented, and a dedicated test bench was designed and manufactured. The test stand consists of:

- The servo drive and the motion controller (as device under test);
- A torque sensor AXIS FSC10 [17], with a 0 Nm to ±10 Nm range and an accuracy of ±0.5 %;
- An adjustable friction clutch KTR Ruflex with a range from 2 Nm to 10 Nm [18];
- A laboratory power supply with voltage ranges from 0 to 50 V and current range from 0 A to 20 A;
- A PC class computer for data acquisition and analysis.

The servo drive and torque sensor are mounted on a common rigid plate. A friction clutch is installed between them. This ensures that the moving system operates under a constant, continuously measured, and angular position-independent load. The angular velocity and angular position of the motor shaft are measured using a Faulhaber IE3-256 incremental encoder, integrated with the electric motor. The motor current is measured by the corresponding motion controller circuit. The data from the motion controller and torque sensor are continuously recorded using Motion Manager [19] and AXIS FM [20] software. The complete test stand is shown in Fig. 6.

A total of 54 test runs were performed for M_{ext} torque values of 0 Nm (disconnected clutch) and from 2 Nm to 8.9 Nm (clutch connected) and motor angular velocities ω_{motor} from 104.7 rad/s to 942.5 rad/s (1000–9000 RPM – Revolutions Per Minute). During each test, the values of $\omega_{motor}\left(t\right)$, $M_{ext}\left(t\right)$, $I_{motor}\left(t\right)$ were measured, and the corresponding $M_{motor.el} = I_{motor} \cdot k_e$ was calculated. The steady-state part of the motion was then extruded from the data at which

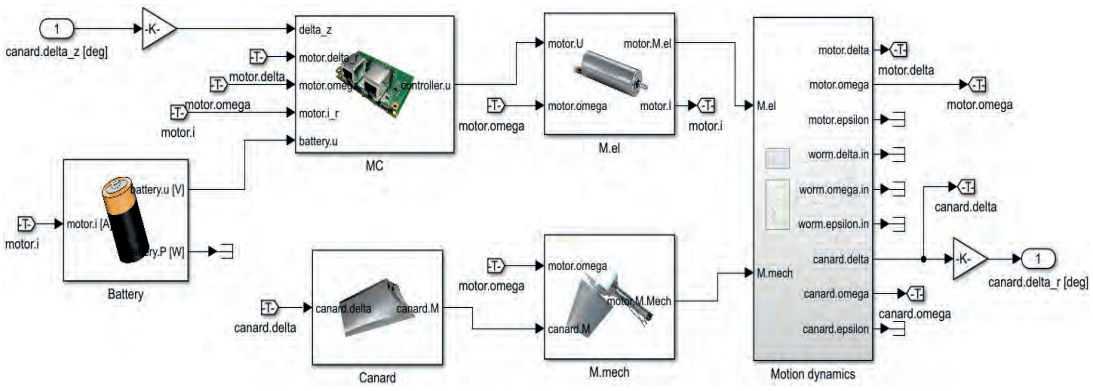

Fig. 5. Model view in Simulink environment
Rys. 5. Widok modelu w środowisku Simulink

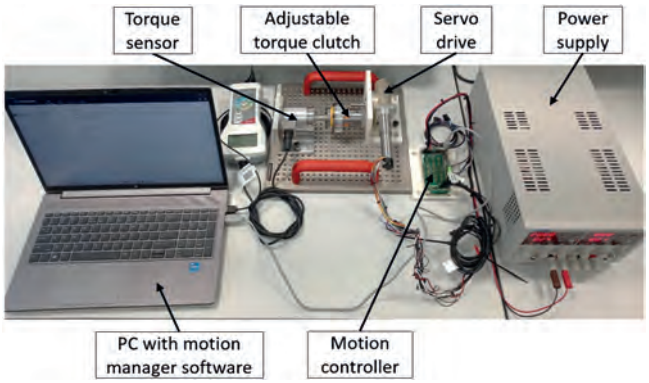

Fig. 6. Test stand for tests with external loads
Rys. 6. Stanowisko badawcze do badań pod obciążeniem zewnętrznym

$\varepsilon_{motor} = 0$, when the moments $M_{motor.el}$ and M_{mech} are in equilibrium ($M_{motor.el} = M_{mech}$). For these ranges of motion, the values obtained were averaged. An example of the measured parameters is shown in Fig. 7.

From the results analyzed this way, a relationship of $M_{mech}\left(\omega_{motor}, M_{ext}\right)$, was obtained, shown in Fig. 8. The results

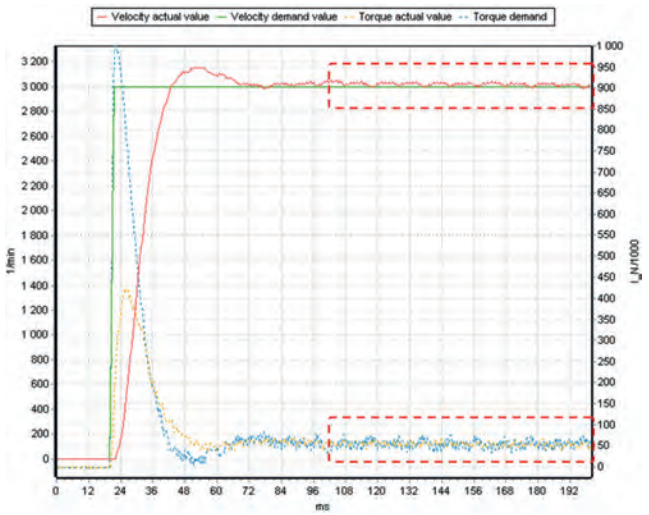

Fig. 7. Example of recorded data. A steady-state part is marked by a red dashed box
Rys. 7. Przykład zarejestrowanych danych. Część ustaloną oznaczono czerwoną przerywaną ramką

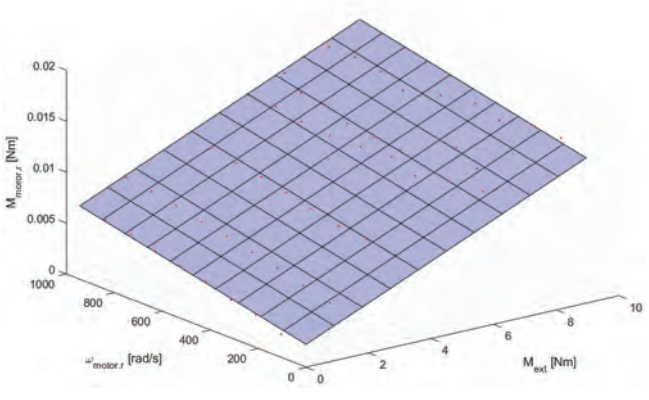

Fig. 8. Results obtained during the test
Rys. 8. Wyniki uzyskane podczas badań

were approximated by a surface formula $M_{mech} = a_1 + a_2 \cdot \omega_{motor} + a_3 \cdot M_{ext}$. The coefficients a_1, a_2 and a_3 obtained from the approximation correspond to C_0, C_v, and C_M and are the required result. The values obtained are shown in Table 1.

Table 1. Summary of obtained results
Tabela 1. Podsumowanie uzyskanych wyników

coefficient	value	unit	% contribution at $M_{ext.\max}$ & $\omega_{motor.\max}$
C_0	$2.25 \cdot 10^{-3}$	[Nm]	12.6 %
C_v	$5.25 \cdot 10^{-6}$	$\left[\frac{\text{Nm}}{\text{rad / s}}\right]$	27.6 %
C_M	$1.34 \cdot 10^{-3}$	$\left[\frac{\text{Nm}}{\text{Nm}}\right]$	59.8 %

4. Results analysis

A summary of all the results obtained during the tests is shown in Table 1. A percentage of contribution for each factor in the total torque have been also calculated in a case of maximal load $M_{ext} = 8$ Nm and maximal angular velocity $\omega_{motor} = 942.5$ rad / s.

As can be seen, the major influence on the load on the electric motor is caused by the external torque acting on the canard shaft. Static and dynamic moments, associated with the movement of the components themselves without load, are also a significant factor and together account for about 40 % of the total system load. Their reduction could therefore lead to an improvement of the system efficiency.

A comparison between the results of simulations and experimental bench test was then performed. For this purpose, a set of identification sequences was designed, including step signals and sine signals of various amplitudes and frequencies. The parameters of the motion controller were set identical in the simulation and in reality. The results obtained are shown in Figures 9–11.

As can be seen, the model shows remarkably high convergence with the experimental results in terms of the positions and velocities obtained. The nature of the response to the step and sine wave signal are nearly coincident. In both cases, typical phenomena can be observed, such as velocity saturation in the case of step signal and sine signals at higher frequencies, resulting in a distorted response and a 'sawtooth' form of the position obtained.

The value of the motor current is also modeled with a fairly good accuracy. The overall of the two curves obtained is similar. Characteristic phenomena such as a high current resulting from the acceleration of the system and an increase in the value of the current flowing with an increase in the external load are noticeable in both cases. Differences between the shape of the obtained curves may be due to phenomena not taken into account in the simulation, such as backlash, the more complex nature of real friction or differences in external torque.

The external load in the model has been adapted to correlate as well as possible with real load. In the real system, nonlinearities and torque hysteresis can be observed, which are not present in the model, but which do not significantly affect the system dynamics. An improved external torque system without hysteresis and nonlinearities is planned for future tests.

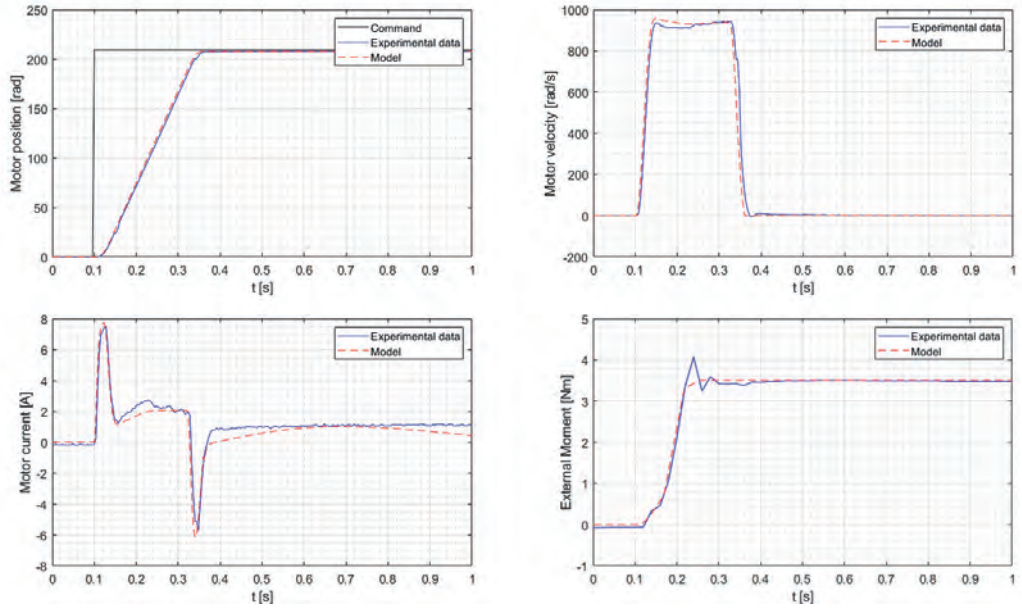

Fig. 9. Comparison between model and experiment – angular step response (5-degree amplitude) – top left: motor position, top right: motor velocity, bottom left: motor current, bottom right: external moment
Rys. 9. Porównanie między modelem i eksperymentem – wychylenie skokowe (amplituda 5 stopni) – na górze po lewej: położenie kątowe silnika, na górze po prawej: prędkość kątowa silnika, na dole po lewej: prąd na silniku, na dole po prawej: moment zewnętrzny

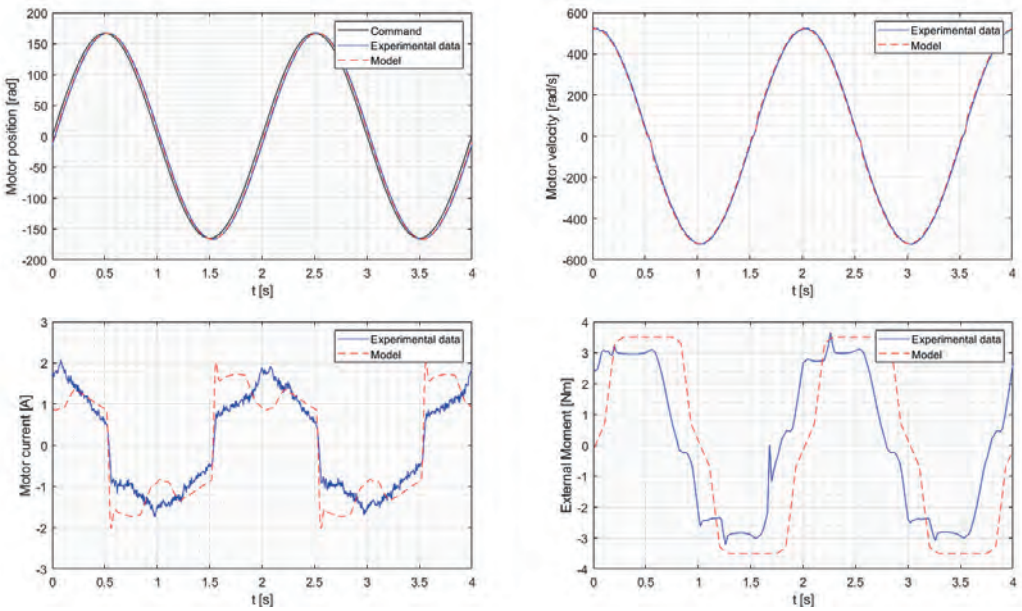

Fig. 10. Comparison between model and experiment – angular sine response (0.5 Hz, 4-degree amplitude) – top left: motor position, top right: motor velocity, bottom left: motor current, bottom right: external moment
Rys. 10. Porównanie między modelem i eksperymentem – wychylenie sinusoidalne (0,5 Hz, amplituda 4 stopnie) – na górze po lewej: położenie kątowe silnika, na górze po prawej: prędkość kątowa silnika, na dole po lewej: prąd na silniku, na dole po prawej: moment zewnętrzny

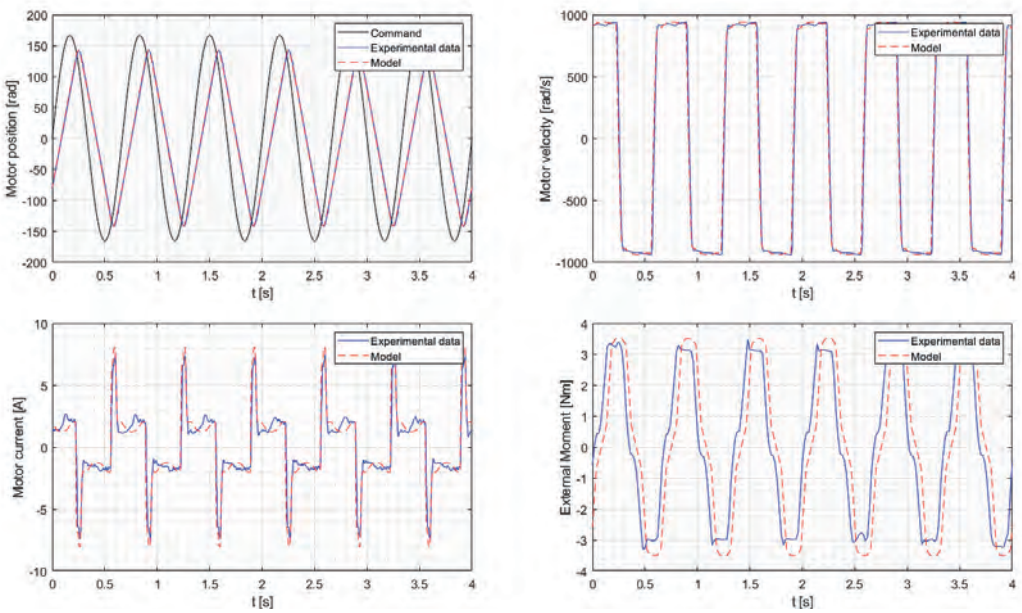

Fig. 11. Comparison between model and experiment – angular sine response (1.5 Hz, 4-degree amplitude) – top left: motor position, top right: motor velocity, bottom left: motor current, bottom right: external moment
Rys. 11. Porównanie między modelem i eksperymentem – wychylenie sinusoidalne (1,5 Hz, amplituda 4 stopnie) – na górze po lewej: położenie kątowe silnika, na górze po prawej: prędkość kątowa silnika, na dole po lewej: prąd na silniku, na dole po prawej: moment zewnętrzny

5. Conclusions

The mathematical model meets its requirements: it reproduces key physical characteristics of the system, such as frequency response and step response time. The model also allows to simulate the system operation without the use of real components. It is then possible to correctly adjust the settings of the control loops, to simulate the effect of physical parameters change on the system's performance, and thus carry out optimisation of the system so that it performs in the desired way. This reduces considerably the time and cost of research and development.

The bench tests permitted to obtain valuable results using relatively inexpensive and easy to use measuring equipment. The results were then used to update the mathematical model. The model updated in this way shows high convergence with experiment for the entire operational range. This confirms the adequacy of the solutions used.

The next development step will consist of coupling the dynamics model of the control system with the flight model of the ILR-33 AMBER rocket and to perform MiL tests simulating selected flight variants. This will be followed by corresponding HiL tests using a prototype system and simulated canard shaft loads. Conducting this type of tests will demonstrate whether the correlation between the whole simulation environment and the real system is at the required level for real flight cases. This will prove whether the system meets the flight requirements regarding trajectory correction and can be qualified for flight tests.

A mechanical and electrical design update of the system is also envisaged. The prototype version of the system described above was designed at a time when detailed aerodynamic and flight analyses of the rocket dynamics had not yet been carried out. Design improvements to the system are therefore necessary due to changes in requirements and relate in particular to the required bandwidth and the aerodynamic forces involved. Despite this, the method developed and demonstrated herein is of great value for the project and will allow the work on future versions to be significantly more efficient.

Acknowledgements

The works are funded by the Łukasiewicz Research Network – Institute of Aviation. Authors are grateful for the support and wish to acknowledge the ILR-33 AMBER project team members involved in the control system development.

References

1. Cieśliński D., Noga T., Pazik A., *Polish civil rockets' development overview*, Obronność RP XXI wieku w teorii i praktyce, Wydawnictwo Lotniczej Akademii Wojskowej, 2021, 61–102.
2. Pakosz M., Noga T., Kaniewski D., Okniński A., Bartkowiak B., *ILR-33 AMBER rocket – quick, low cost and dedicated access to suborbital flights for small experiments*, 24th ESA Symposium on European Rocket and Balloon Programmes and Related Research, Essen, 2019.
3. Noga T., Cieśliński D., Dul S., Umiński P., Dziczkaniec R., Matysek K., *On the Safety of Suborbital Rocket Launches from the Polish Coast*, "Safety & Defense", Vol. 9, No. 1, 2023, 31–46, DOI: 10.37105/sd.199.
4. Kotarski A., *A Concept of Suborbital Scientific Mission and Technology Validation*, "Transactions on Aerospace Research", Nr 3, 2019, 66–74, DOI: 10.2478/tar-2019-0018.
5. Ćosić K., Kopriva I., Kostić T., Slamić M., Volarević M., Design *and implementation of a hardware-in-the-loop simulator for a semi-automatic guided missile system*, "Simulation Practice and Theory", Vol. 7, No. 2, 1999, 107–123, DOI: 10.1016/S0928-4869(98)00027-5.
6. Kim S.H., Tahk M.-J., Lee H.-J., Kim S.-H., *Experimental study on integrated servo control for canard-controlled missiles* [*Correspondence*], "IEEE Transactions on Aerospace and Electronic Systems", Vol. 52, No. 3, 2016, 1467–1474, DOI: 10.1109/TAES.2016.150211.
7. Gurav B., Economou J., Saddington A., Knowles K., *Multi-Mode Electric Actuator Dynamic Modelling for Missile Fin Control*, "Aerospace", Vol. 4, No. 2, 2017. DOI: 10.3390/aerospace4020030.
8. Campa R., Torres E., Salas F., Santibáñez V., *On Modeling and Parameter Estimation of Brushless DC Servoactuators for Position Control Tasks*, "IFAC Proceedings Volumes", Vol. 41, No. 2, 2008, 2312–2317, DOI: 10.3182/20080706-5-KR-1001.00390.
9. Czerwiński E., Olejnik P. Awrejcewicz J., *Modeling And Parameter Identification Of Vibrations Of A Double Torsion Pendulum With Friction*, "Acta Mechanica et Automatica", Vol. 9, No. 4, 2015, 204–212, DOI: 10.1515/ama-2015-0033.
10. Skjetne R., Egeland O., *Hardware-in-the-loop testing of marine control system*, "Modeling", Vol. 27, No. 4, 2006, 239–258, DOI: 10.4173/mic.2006.4.3.
11. Yong-guang L., Qin L., *Design of the Test Platform of Servo System*, Proceedings of the 1st International Conference on Mechanical Engineering and Material Science, 2012, 203–205, DOI: 10.2991/mems.2012.55.
12. Andersson S., Söderberg A., Björklund S., *Friction models for sliding dry, boundary and mixed lubricated contacts*, "Tribology International", Vol. 40, No. 4, 2007, 580–587, DOI: 10.1016/j.triboint.2005.11.014.
13. Sahbon N., Murpani S., Michałów M., Miedziński D., Sochacki M., *A CFD Study of the Aerodynamic Characteristics of Twardowsky and FOK Rockets*, "Transactions on Aerospace Research", No. 1, 2022, 35–58, DOI: 10.2478/tar-2022-0003.

Other sources

14. *Faulhaber technical manual nr 7000.05048*, 2019.
15. *Brushless DC-Servomotors*, [www.faulhaber.com/en/products/series/2264bp4].
16. *Planetary Gearheads Series 26/1R*, [www.faulhaber.com/en/products/series/261r].
17. AXIS, *FSC10*, [www.axis.pl/pl/fsc/454-fsc10.html].
18. KTR, *Sprzęgło ślizgowe RUFLEX z elastomerem ROTEX*, [www.ktr.com/pl/produkty/ruflex-sprzegla-slizgowe-piasty-slizgowe/ruflex-z-rotex/].
19. *FAULHABER Motion Manager*, [www.faulhaber.com/en/support/faulhaber-motion-manager/].
20. AXIS, *AXIS Darmowe Oprogramowanie*, [www.axis.pl/pl/73-darmowe].

Modelowanie i identyfikacja siłowników elektromechanicznych do rakiety ILR-33 BURSZTYN

Streszczenie: Celem artykułu było przedstawienie metody modelowania, testowania i identyfikacji siłowników elektromechanicznych do zastosowań rakietowych. Prace przeprowadzono z użyciem prototypowego rozwiązania, zaprojektowanego do rakiety suborbitalnej ILR-33 BURSZTYN, rozwijanej przez Sieć Badawczą Łukasiewicz – Instytut Lotnictwa. Do zbudowania modelu matematycznego systemu wykorzystano zestaw zależności fizycznych, w tym prawa Kirchhoffa, prawa Newtona i nieliniowe modele tarcia. Następnie przeprowadzono badania eksperymentalne układu. Przedstawiona tu nowa metoda analizy wyników badań pozwoliła na pozyskanie brakujących danych do modelu i na uzyskanie wysokiej zbieżności pomiędzy modelem i eksperymentem nimi we wszystkich analizowanych przypadkach. Tym samym wykazano, że przedstawione tu podejście jest efektywne i użyteczne. W artykule po raz pierwszy zaprezentowano kompleksowe podejście do tematu modelowania, badania i identyfikacji tego typu siłowników. Przedstawione tu rozwiązania mogą być zaaplikowane w innych dziedzinach, w których wykorzystywane są siłowniki elektromechaniczne oraz gdzie ich poprawna identyfikacja jest konieczna do zapewnienia niezawodności i bezpieczeństwa pracy systemu. Przedstawione podejście jest proste w implementacji, a stanowiska badawcze nie wymagają kosztownego oprzyrządowania pomiarowego. Otrzymane wyniki pozwalają na stworzenie wiarygodnego modelu o racjonalnie niskim koszcie obliczeniowym.

Słowa kluczowe: rakieta suborbitalna, ILR-33 BURSZTYN, modelowanie, identyfikacja, siłownik elektromechaniczny, serwomechanizm, system sterowania

Jan Kierski, MSc Eng.
jan.kierski@ilot.lukasiewicz.gov.pl
ORCID: 0000-0001-7361-6277

Received his MSc degree in aerospace engineering in 2018. Currently a PhD student at Warsaw University of Technology. Since 2014 involved in rocketry projects for education, civil and military purposes. Since 2020 working for the Lukasiewicz Research Network – Institute of Aviation and developing the ILR-33 AMBER suborbital rocket. His research interests include mechanical design, control systems design, modeling, and simulation of dynamical systems, as well as system engineering and project management activities. In his spare time, an enthusiast of athletics and cooking.

Hubert Graczyk, MSc Eng.
hubert.graczyk@ilot.lukasiewicz.gov.pl
ORCID: 0009-0000-1219-3303

Graduated in Automation and Robotics at the Faculty of Electrical Engineering, Warsaw University of Technology, received his MSc degree in 2021. Currently employed at the Lukasiewicz Research Network - Aerospace Institute as an electronics engineer. His professional research focuses on aerospace avionics and rocket technologies. Interested in high reliability electrical devices for harsh environment applications, robotics, and autonomous vehicles. As a hobbyist, involved in the design of an electric vehicle adapted to a person with mobility disabilities.